Biochimie 95 (2013) 2168–2176

Contents lists available at ScienceDirect

Biochimie

journal homepage: www.elsevier.com/locate/biochi

Research paper

Ultrafast interfacial solvation dynamics in specific protein DNA recognition

Subrata Batabyal [a], Tanumoy Mondol [a], Susobhan Choudhury [a], Abhishek Mazumder [b], Samir Kumar Pal [a,*]

[a] Department of Chemical, Biological & Macromolecular Sciences, S.N. Bose National Centre for Basic Sciences, Block JD, Sector III, Salt Lake, Kolkata 700 098, India
[b] Waksman Institute of Microbiology, 190 Frelinghuysen Road, Piscataway, NJ 08854, USA

ARTICLE INFO

Article history:
Received 12 June 2013
Accepted 6 August 2013
Available online 20 August 2013

Keywords:
Specific protein DNA interaction
Protein DNA interface
Operator DNA
DNA minor groove water dynamics
Resonance energy transfer

ABSTRACT

An overwhelming number of structural and functional studies on specific protein–DNA complexes reveal the existence of water molecules at the interaction interface. What role does the interfacial water molecules play in determining the specificity of association is thus a critical question. Herein, we have explored the dynamical role of minor groove water molecules and DNA side chain flexibility in lambda repressor–operator DNA interaction using well-characterized DNA minor groove binder dye, Hoechst 33258. The most striking finding of our studies reveals that the solvation time scale corresponding to the minor groove water molecules (~50 ps) and DNA side chain flexibility (~10 ns) remain unaltered even in protein–DNA complex in comparison to unbound operator DNA. The temperature dependent study further reveals the slower exchange of minor grove water molecules with bulk water in DNA–protein complex in comparison to the unbound DNA. Detailed structural studies including circular dichroism (CD) and Förster resonance energy transfer (FRET) have also been performed to elucidate the interaction between protein and DNA.

1. Introduction

Interaction of regulatory DNA binding protein with their target sites is responsible for the regulation of key biological functions such as gene expression [1], DNA repair and recombination [2], signal transduction [2,3] etc. The functional perspective of a protein–DNA complex is critically dictated by the static and dynamic aspects of the conformation of protein and DNA in complex. Specific protein–DNA interaction [4] is governed by sequence recognition (base readout) through direct contacts between protein's amino acid side chains and DNA bases [5], as well as the spatial geometry of the two biomolecules (shape readout) [5]. Non-specific protein–DNA interaction [2,6] however is governed by purely electrostatic forces [7] of interaction between the negatively charged DNA and the protein and does not have sequence dependence. In contemporary literature, there are ample examples of studies dealing with such specific/non-specific protein–DNA interaction enlightening the driving force for the interactions, role of solvent molecules, and the involved thermodynamics [8–12]. In protein–DNA complex formation, proteins interact with both major and minor grooves of DNA, *via* hydrogen bonding and hydrophobic interactions as well as water-mediated interactions [13]. Most structural and functional studies on different specific protein–DNA complexes reveal the existence of water molecules at the interaction interface [14]. The important contribution of these interfacial water molecules to the stability and specificity of protein–DNA interactions has been recognized through a combination of high-resolution structural and allied computational studies [15–17]. Several such studies indicate towards different roles of water molecules that act as a screen to neutralize like charges on proteins and DNA, enabling formation of water mediated hydrogen bonds. However, these structural (mainly crystallography and NMR) and theoretical studies do not cover the aspects of the dynamics of water molecules bound to the DNA in the complex [18,19].

In this context, we have exploited the unique opportunity to study a model protein–DNA complex comprising of lambda repressor (λ-repressor) protein and the two operator DNA sites, O_R1 and O_R2. Structurally λ-repressor is a two-domain protein, the N-terminal domain interacts with the operator DNA, while C-terminal domain is responsible for most protein–protein interactions, these interactions are essential for the co-operative

* Corresponding author.
E-mail address: skpal@bose.res.in (S.K. Pal).

0300-9084/$ – see front matter © 2013 Elsevier Masson SAS. All rights reserved.
http://dx.doi.org/10.1016/j.biochi.2013.08.015

binding and for the functioning of the genetic switch [20]. These target operator DNA sites are 17 base pairs pseudo-palindromic sites bearing close similarity with each other [21]. The repressor protein interacts with different operator DNA with differing specificity [20,22–25]. The exploration of the dynamical role of minor groove water molecules in specific protein–DNA interaction is one of the main motives of our present work. Though various structural studies demonstrated the presence and importance of water molecules in the specific protein–DNA interface, the dynamical time scales at the interface are very sparse in the literature. In addition, we intend to explore the change of DNA backbone flexibility in the protein–DNA complex. In order to unravel the role of minor groove water dynamics and DNA side chain motion in the specific protein–DNA interaction, we have used a well-known fluorescent probe, Hoechst 33258 (H258). The cationic nature and minor groove matching concaveness allow H258 to interact with the DNA minor grooves through van der Walls force and hydrogen bonding [26]. Earlier femtosecond-resolved solvation studies on H258 bound to DNA minor groove revealed sub-100 ps water relaxation time [19]. On the other hand, long time component (~ns) is reported to be associated to the DNA backbone flexibility [27]. In the present context, our picosecond-resolved solvation dynamics study of H258 provides a unique opportunity to explore both minor groove water relaxation (ps time scale) and the DNA side chain flexibility (ns time scale).

The physical characterization of the binding nature of the probe and the conformation of the DNA structure before and after interaction with protein was elucidated with the help of steady-state/time-resolved fluorescence spectroscopy, circular dichroism, and time-resolved fluorescence anisotropy studies. Detailed Förster resonance energy transfer analysis was carried out in order to investigate the conformational perturbation of the DNA in the complex. Picosecond-resolved lifetime traces of H258 were analyzed to estimate the dynamical behavior of water molecules present in the DNA minor grooves and the flexibility of the DNA side chain. The stability of minor groove water molecules and the dynamical exchange of such water molecules with the bulk water molecules were further investigated through temperature dependent solvation studies in the DNA–protein complex.

2. Materials and methods

2.1. Chemicals

Acrylamide, isopropyl β-D-thiogalactopyranoside (IPTG), ampicillin, Coomassie brilliant blue, poly(ethyleneimine) and phenylmethanesulfonylfluoride (PMSF) were purchased from Sigma Chemical Co. (St. Louis, MO). Bacto-tryptone, bacto-agar, and yeast extract were purchased from Difco Laboratories (Detroit, MI). β-Mercaptoethanol and glycerol were purchased from Aldrich Chemical Co. (Milwaukee, WI). Hoechst 33258 (*p*-(5-(5-(4-methyl-1-piperazinyl)-1*H*-2-benzimidazolyl)-1*H*-2-benzimidazolyl) phenol) and ethidium bromide(3,8-diamino-5-ethyl-6-phenylphenanthridinium bromide) were purchased from Molecular Probes Inc. All other reagents were of analytical grade quality. O_R1 (5′CGTACCTCTGGCGG TGATAG3′) and its complementary oligonucleotide, O_R2 (5′GACAAC ACGCACGGTGTTGC3′) and its complementary oligonucleotide were purchased from Trilink (USA). The concentrations of DNA were calculated from the absorbance value at 260 nm, using extinction coefficient for purine to be $14 \times 10^3\ M^{-1}\ cm^{-1}$ and that for pyrimidine to be $7 \times 10^3\ M^{-1}\ cm^{-1}$. The oligonucleotides mixed at 1:1 molar ratio were annealed in annealing buffer (10 mM Tris, pH 7.5–8.0, 50 mM NaCl, 1 mM EDTA) by heating at 90 °C and then cooling slowly to room temperature.

2.2. Repressor isolation

λ-Repressor was isolated from a strain of *Escherichia coli* RR1 15 Δlac Z carrying a plasmid pEA305, which contains the wild type *cI* gene under the control of *tac* promoter. The details of the purification procedure have been elaborated elsewhere [28]. The native repressor concentration was determined using extinction coefficient of 26,300 $M^{-1}\ cm^{-1}$ at 280 nm. Molar concentration of the repressor was always calculated in terms of dimer subunit as in our experimental concentration, λ-repressor exists predominantly in dimeric form in lower concentration [29] consisting of two identical subunits [30]. For all studies, the repressor was dialyzed against 0.1 M potassium phosphate buffer, pH 8.0.

2.3. Steady state spectroscopy

All absorbance measurements were performed in a Shimadzu UV-2450 spectrophotometer. All fluorescence measurements were performed in a Jobin Yvon Fluoromax-3 fluorimeter. Concentrations of H258, DNA and repressor in the experiments were kept at 1.5 μM, 3.0 μM and 3.0 μM respectively. Assuming one molecule of ethidium lying between four base pairs of DNA, the concentration of EtBr was chosen accordingly. All the samples were prepared in 0.1 M phosphate buffer at pH 8. For performing the fluorescence measurement, the bandwidth of excitation and emission slits were kept at 5 nm.

2.4. CD measurement

Circular dichroism (CD) measurements were done on a JASCO J850 spectropolarimeter using a 1 cm path length quartz cuvette, following the procedures reported earlier [31]. The CD spectra of DNA and DNA–protein complex were taken at oligonucleotide concentrations of 0.25 μM and protein concentrations of 1.0 μM, respectively. The buffer-only spectrum was subtracted from the oligonucleotide spectrum, and the protein-only spectrum was subtracted from the complex spectra. The difference between the DNA and protein bound DNA was qualitatively estimated by the difference in CD (mdeg) value between the two spectra at a wavelength of 270 nm.

2.5. Time-resolved spectroscopy

Time-resolved studies were performed with a time correlated single photon counting (TCSPC) setup from Edinburgh Instruments. A picosecond pulsed laser diode was used to excite the sample at 375 nm having Instrument response function (IRF) of 70 ps. The excitation was vertically polarized, and the emission was recorded through a polarizer oriented at 55° from the vertical position. Incorporation of a long-pass filter with a cut off at 400 nm in the emission channel effectively eliminates possible scattered excitation light. The picosecond-resolved fluorescence transients were fitted with multi-exponential (n) function, $\sum_{i=1}^{n} A_i \exp(-t/\tau_i)$ where, A_i's are weight percentages of the decay components with time constants of τ_i. The average excited state lifetime is expressed by the equation $\tau = \sum_{i=1}^{n} A_i \tau_i$, when $\sum_{i=1}^{n} A_i = 1$.

The Förster distances of donor–acceptor pair were calculated using the equation [32],

$$R_0 = 0.211 \times \left[\kappa^2 n^{-4} \Phi_D J(\lambda)\right]^{\frac{1}{6}} In\ (\text{Å}) \quad (1)$$

where, R_0 is the distance between the donor and the acceptor at which the energy transfer efficiency is 50%, κ^2 is a factor describing the relative orientation in space of the transition dipoles of the donor and acceptor. The magnitude of κ^2 is assumed to be 0.66 for

random orientation of donor and acceptor pair. However, in DNA, for one dimensional geometry, the orientation factor for dipole–dipole interaction is assumed to be 1.25 [33]. The refractive index (n) of the medium (biological systems) is assumed to be 1.4 [32]. $J(\lambda)$, the overlap integral, which expresses the degree of spectral overlap between the donor emission and the acceptor absorption, is given by,

$$J(\lambda) = \frac{\int_0^\infty F_D(\lambda)\varepsilon_A(\lambda)\lambda^4 \mathrm{d}\lambda}{\int_0^\infty F_D(\lambda)\mathrm{d}\lambda} \tag{2}$$

where, $F_D(\lambda)$ is the fluorescence intensity of the donor in the wavelength range of λ to $\lambda + d\lambda$ and is dimensionless. $\varepsilon_A(\lambda)$ is the extinction coefficient (in M^{-1} cm^{-1}) of the acceptor at λ. If λ is in nm, then $J(\lambda)$ is in units of M^{-1} cm^{-1} nm^4. Once the value of R_0 is known, the donor–acceptor distance (r) can easily be calculated using the formula:

$$r^6 = \left[R_0^6(1-E)\right]/E \tag{3}$$

Here, E is the efficiency of energy transfer, which can be expressed as follows,

$$E = 1 - \frac{\tau_{DA}}{\tau_D} \tag{4}$$

where τ_D and τ_{DA} are lifetimes of the donor in absence and in presence of the acceptor.

For anisotropy ($r(t)$) measurements, emission polarization was adjusted to be parallel or perpendicular to that of the excitation light and anisotropy is defined as,

$$r(t) = \frac{[I_{\mathrm{para}} - G \times I_{\mathrm{perp}}]}{[I_{\mathrm{para}} + 2 \times G \times I_{\mathrm{perp}}]} \tag{5}$$

G, the grating factor is determined following tail matching technique and found out to be nearly 1.5 [34]. The time-resolved anisotropy of a probe reveals the physical motion of the probe in a microenvironment. The time constants reflect rotational correlation time of the probe in the microenvironment.

To construct time resolved emission spectra (TRES), we followed the technique described in literature [32,35]. The time dependent fluorescence Stoke's shifts, as estimated from TRES, were used to construct the normalized spectral shift correlation function or the solvent correlation function $C(t)$ defined as,

$$C(t) = \frac{\nu(t) - \nu(\infty)}{\nu(0) - \nu(\infty)} \tag{6}$$

where $\nu(0)$, $\nu(t)$, and $\nu(\infty)$ are the emission maxima (in cm^{-1}) at time 0, t, and ∞, respectively. The $\nu(\infty)$ values have been taken to be the emission frequency beyond which insignificant or no spectral shift is observed. The $C(t)$ function represents the temporal response of the solvent relaxation process, as occurs around the probe following its photo-excitation and the associated change in the dipole moment.

2.6. Tachiya kinetic model

We have applied a kinetic model developed by Tachiya for the quenching of luminescent probes in micelles [36]. The decay of excited state of probes in such host medium may be described by the following kinetic model, which is known as the Tachiya model:

$$P_n^* \xrightarrow{k_0} P_n \tag{7}$$

$$P_n^* \xrightarrow{nk_q} P_n \tag{8}$$

where P_n^* stands for a host molecule containing an excited state probe and n no of quencher molecules, while P_n stands for a host molecule which contains n no of quencher molecules at ground state. k_0 is the total decay constant of the probe in excited state in absence of a quencher. k_q is the rate constant for quenching of an excited state probe in a host molecule containing one quencher molecule. In this kinetic model, it is assumed that the distribution of the number of quenchers attached to one host molecule follows a Poisson distribution [36], namely,

$$p(n) = (m^n/n!)\exp(-m) \tag{9}$$

where m is the mean number of quenchers in a host molecule.

$$m = k_+[A]/k_- \tag{10}$$

where k_+ is the rate constant for entry of a quencher molecule into a host molecule, while k_- is the rate constant for exit of a quencher molecule from a host molecule containing one quencher molecule. $[A]$ stands for the concentration of quencher molecule in the aqueous phase. Based upon the above model, the equation for the total concentration $P^*(t)$ of excited state probes at time t is given by [36]:

$$P^*(t) = P^*(0)\exp\left[-\left(k_0 + \frac{k_0 k_+[A]}{k_- + k_q}\right)t - \frac{k_q^2 k_+[A]}{k_-(k_- + k_q)^2} \times \{1 - \exp[-(k_- + k_q)t]\}\right] \tag{11}$$

If k_- is much smaller than k_q, equation (11) reduces to,

$$P^*(t) = P^*(0)\exp\{-k_0 t - m[1 - \exp - (k_q t)]\} \tag{12}$$

The model relies upon two assumptions [36], the first one considers no limit to the number of solubilized molecules in any of the micelle, and there is no variation in the entry rate constant (k_+) with the number of solubilized molecules already present. The second assumption considers that when a micelle contains n solubilized molecules, the rate constant for exit of a solubilized molecule from the micelle is n times as fast as when it contains one solubilized molecule. In recent past the model has been successfully used to understand the drug binding to polymer degradation [37], nanoparticle quenching [38] etc. The above model is well relevant in our experimental framework. In our system, DNA acts as host entity where the quencher, ethidium resides. We have determined the values of the parameters m, k_q and k_0 by fitting the decay curves of the donor (H258) in the excited state in the absence and presence of increasing concentration of quencher molecule (EtBr) to the equation (12). The observed fluorescence transients were fitted using a nonlinear least squares fitting procedure (software SCIENTIST™) to a function ($X(t) = \int_0^t E(t')P(t-t')\mathrm{d}t'$) comprising of the convolution of the IRF ($E(t)$) with exponential $[P^*(t) = P^*(0)\exp\{-k_0 t - m[1 - \exp(-k_q t)]\}]$.

2.7. Distance distribution in donor–acceptor systems

Distance distribution between donor and acceptor was estimated according to the procedure described in the literature [32,39]. The observed fluorescence transients of the donor (H258) in absence of acceptor (EtBr) in DNA and DNA–protein complex were fitted using a nonlinear least-squares fitting procedure (software SCIENTIST™) to the following function,

$$I_D(t) = \int_0^t E(t')P(t'-t)\mathrm{d}t' \tag{13}$$

which comprises the convolution of the IRF ($(E(t))$) with exponential ($P(t) = \sum_i \alpha_{Di}\exp(-t/\tau_{Di})$). The distance distribution function $P(r)$ in the fluorescence transients of donor in presence of acceptor in the system under studies is estimated using the same software (SCIENTIST™) in the following way.

The intensity decay of D–A pair, spaced at a distance r, is given by

$$I_{DA}(r,t) = \sum_i \alpha_{Di}\exp\left[-\frac{t}{\tau_{Di}} - \frac{t}{\tau_{Di}}\left(\frac{R_0}{r}\right)^6\right] \tag{14}$$

and the intensity decay of the sample considering $P(r)$ is given by

$$I_{DA}(t) = \int_{r=0}^{\infty} P(r)I_{DA}(r,t)\mathrm{d}r \tag{15}$$

Where $P(r)$ consist of the following terms:

$$P(r) = \frac{1}{\sigma\sqrt{2\pi}}\exp\left[-\frac{1}{2}\left(\frac{\bar{r}-r}{\sigma}\right)^2\right] \tag{16}$$

In this equation $\bar{r}$ is the mean of the Gaussian with a standard deviation of σ. Usually distance distributions are described by the full width at half maxima and half width is given by $hw = 2.354\sigma$.

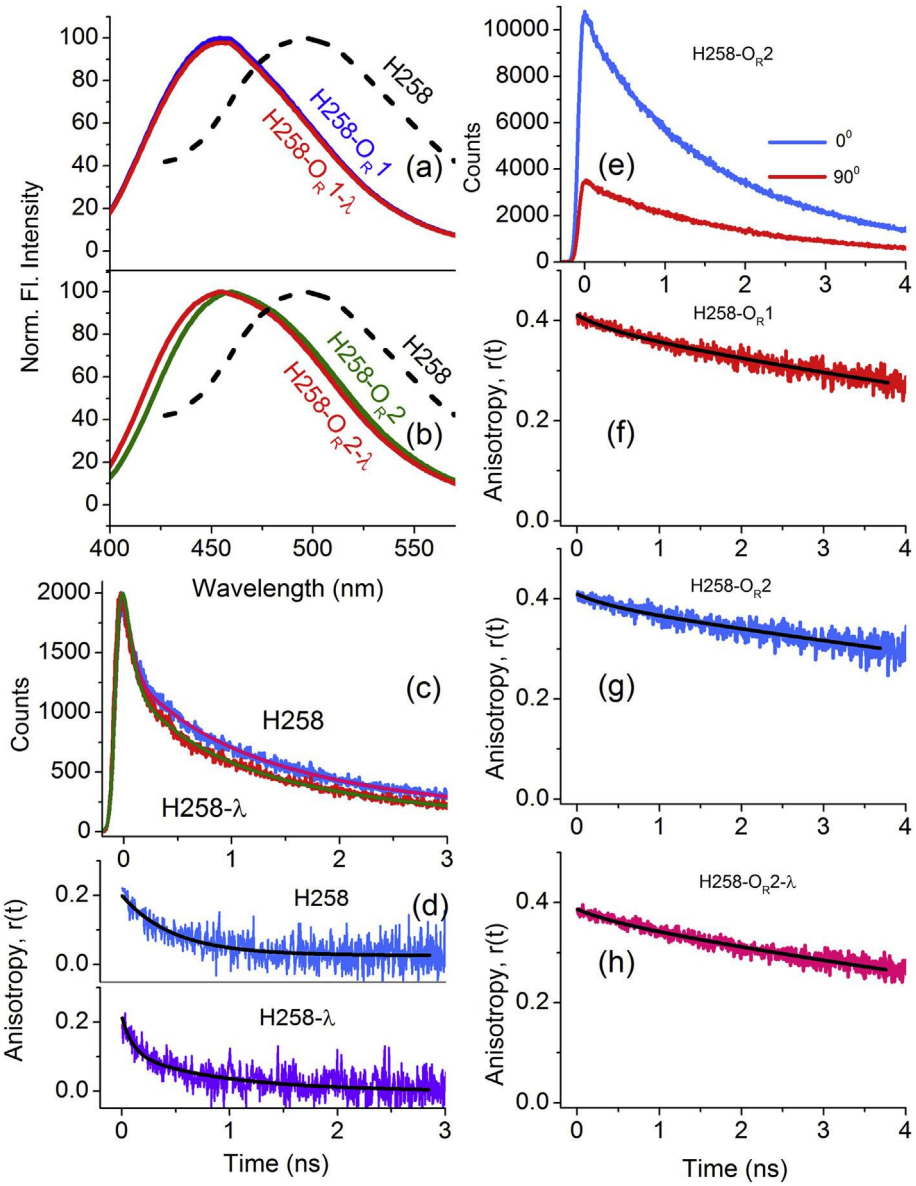

Fig. 1. Normalized steady-state fluorescence spectra of probe H258 in three different environments: (a) in buffer, O_R1 DNA and O_R1–repressor complex, (b) in buffer, O_R2 DNA and O_R2–repressor complex. (c) Picosecond-resolved fluorescence transients of H258 are shown in presence and absence of λ-repressor protein. For comparison, the fluorescence transient of H258 in buffer solution is also included. (d) Time-resolved fluorescence anisotropies, $r(t)$, of the probe in water (buffer) and in presence λ-repressor protein at emission wavelength of 500 nm are shown. (e) Representative time-resolved traces of H258 in O_R2 at different polarization (0° and 90°) is shown. Time-resolved fluorescence anisotropies of H258 in O_R1 (f) and O_R2 (g) are depicted. (h) Represents the anisotropy decay of H258 in O_R2-protein complex.

3. Results and discussion

3.1. Structural studies

Fig. 1a,b show emission spectra of Hoechst 33258 (H258) bound to different operators DNA in presence and absence of λ-repressor. In presence of O_R1 and O_R2 DNA, the emission maximum of H258 (buffer: 500 nm) is significantly blue shifted (O_R1 DNA: 457 nm, O_R2 DNA: 460 nm) due to the interaction of H258 with DNA. Upon addition of λ-repressor to the H258, bound to operator DNA, the emission spectrum is further blue shifted especially in H258–O_R2–λ complex as shown in Fig. 1b. From the steady-state experiments, it is evident that upon repressor binding, the local environment around H258 in O_R2 DNA (Fig. 1b) is influenced to a greater extent in comparison to O_R1 DNA (Fig. 1a). To rule out the possibility of any specific interaction between H258 and λ-repressor leading to such spectral change, a set of control time-resolved experiments were carried out. From the fluorescence lifetime transients (Fig. 1c), it is evident that the non-specific binding of H258 with repressor is insignificant as the lifetime of H258 is minimally perturbed in presence of repressor. Time-resolved polarization gated fluorescence anisotropy analysis (Fig. 1d) further supports the observation as the rotational time constant (τ_{rot}) of H258 in absence and in presence of λ-repressor remains unaltered ($\tau_{rot} = 0.55$ ns). The anisotropy decay constant of ~0.55 ns is indicative of the free rotational motion of the probe in aqueous solution [40]. The fluorescence anisotropy decays of H258 in presence of O_R1 and O_R2 DNA are presented in Fig. 1f and g. The representative time-resolved fluorescence intensity decays at different polarization (0° and 90°) for H258–O_R2 complex are presented in Fig. 1e. The bi-exponential anisotropy decay of H258 in O_R1 and O_R2 are quite similar. In case of O_R1, the rotational decay consists of 0.4 ns and 10 ns decay components, whereas, in case of O_R2, the rotational decay consists of 0.4 ns and 14 ns decay components. The details of anisotropy data are provided in Table 1. It has to be noted that the fluorescence anisotropy decays were collected at the corresponding emission maxima of the concerned systems. In DNA–protein complex, the anisotropy decay pattern of H258 remains unaltered, suggesting the location of the probe in DNA does not change even after the complex formation. The representative anisotropy decay of H258 in DNA–protein complex is shown in Fig. 1h.

The steady-state fluorescence measurements and time-resolved fluorescence anisotropy decays reveal the binding nature of H258 to the operator DNA in absence and presence of repressor. In order to investigate conformational and structural changes of the operator DNA, upon interaction with λ-repressor, circular dichroism (CD) spectroscopy was used. Fig. 2 represents the CD spectra of operator DNA, O_R1 and O_R2 in absence and in presence of λ-repressor. In case of O_R2 (Fig. 2b), careful observation reveals a shift of the spectral maximum (270 nm) along with the increase in ellipticity upon complexation with λ-repressor. In case of O_R1 DNA (Fig. 2a), negligible spectral shift and smaller change in ellipticity was observed in comparison to O_R2. The observation indicates the conformational change of O_R2 after binding to the repressor is significant compared to that of O_R1. The inset of Fig. 2a represents the CD spectrum of unbound λ-repressor, indicating no possible interference of CD signal at 270 nm wavelength. The characteristic wavelength shift in the CD spectra of operator DNA (O_R2) upon repressor binding is consistent with the reported protein induced bending of DNA [41].

To further investigate the structural aspects of DNA and its change upon protein binding, we carried out Förster resonance energy transfer (FRET) study from DNA bound H258 to ethidium moieties intercalated into DNA. Steady-state emission quenching of DNA bound H258 in presence of EtBr is evident in Fig. 3a. In an earlier study, we have shown that H258 and EtBr can bind simultaneously to DNA, without displacing each other [42]. In that study, it was also demonstrated that H258 and EtBr serve as an excellent FRET pair, where H258 is an energy donor and EtBr is an energy acceptor. The time-resolved fluorescence transients are represented in Fig. 3b. As evident, from Fig. 3b (lower panel), upon addition of repressor to O_R2, the efficiency of energy transfer from H258 to EtBr decreases (72%–59%), whereas in case of O_R1 (upper panel), the efficiency remains unaltered (57%). The FRET study clearly demonstrates that O_R2 DNA undergoes significant conformation change upon protein binding, leading to the decrease in energy transfer efficiency. From the calculated R_0 value (3.81 nm) and measured FRET efficiency, the donor (H258)–acceptor (EtBr) distance in O_R1 and O_R2 was estimated as 3.58 nm and 3.25 nm respectively. Upon addition of λ-repressor, the donor–acceptor distance in O_R2–repressor complex reveals value of 3.6 nm. The change in orientation factor between donor and acceptor dipoles could also contribute to the decrease in the energy transfer

Table 1
Bi-exponential anisotropy decay fitting of H258 in operator DNA and DNA–protein complex.

System	τ_1 (ns) %	τ_2 (ns) %	τ_{rot} (ns)
H258–O_R1	0.44 (5%)	10 (95%)	9.53
H258–O_R1–λ	0.41 (5%)	10 (95%)	9.52
H258–O_R2	0.43 (4%)	14 (96%)	13.45
H258–O_R2–λ	0.43 (4%)	14 (96%)	13.45

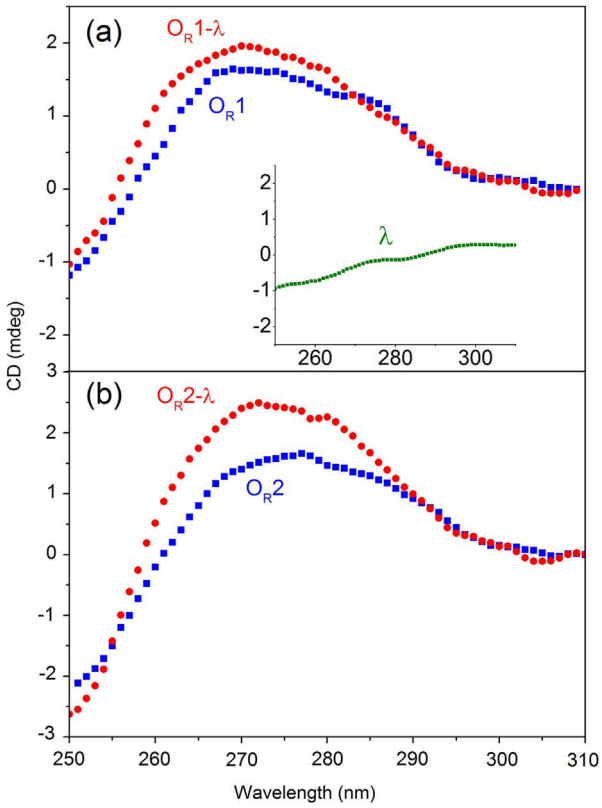

Fig. 2. (a) Ellipticity (mdeg) of O_R1 DNA in presence and in absence of λ-repressor protein. The inset figure represents the CD spectrum of λ-repressor protein. (b) Depicts the optical rotation (mdeg) of O_R2 DNA in presence and in absence of λ-repressor protein. Upon complexation with protein, the characteristic peak of DNA around 270 nm is blue shifted. No significant wavelength shift was observed in case of O_R1.

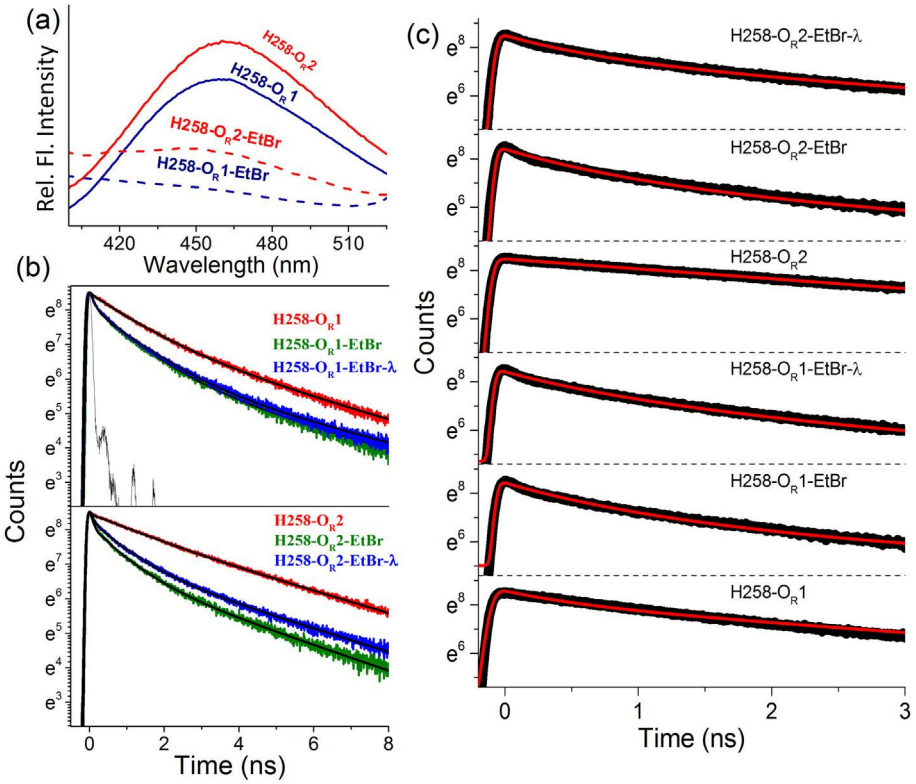

Fig. 3. (a) Steady-state emission spectra of H258 in operator DNA in presence and in absence of EtBr. (b) The fluorescence lifetime quenching of H258. Upper panel shows the effect of EtBr in O_R1 system and the lower panel depicts the energy transfer for O_R2 system. (c) Fitting of time-resolved lifetime data of H258 under various conditions by Tachiya kinetic model.

efficacy, in addition to the change in donor–acceptor distance. The observation corroborates the findings of the CD study, which also indicates the structural changes within O_R2 DNA. For better understanding of the energy transfer from the excited state of H258 to EtBr molecules, it is imperative to know the distribution of acceptor (EtBr) molecules within the DNA, as it is a governing factor that can influence the energy transfer rate as observed from the time resolved fluorescence studies [43]. In this context, we have applied a kinetic model developed by Tachiya [44] for the quenching of luminescent probes undergoing non-radiative energy transfer in restricted environments. In contemporary literature, the kinetic model finds its relevance in various aspects including drug binding [45], nanoparticles quenching [38]. The model provides a clear understanding about the number of possible binding sites of the host molecules. In our case, the host being the DNA strand itself, where EtBr intercalates. For O_R1 DNA (Fig. 3c), the mean number (m) of intercalated ethidium moiety present per DNA was estimated to be ~5 and the quenching rate constant (k_q) was estimated 0.9 ns^{-1}. The m and k_q values remain unchanged in DNA–protein complex. In case of O_R2 (Fig. 3c), the mean number of acceptor (ethidium) per DNA was estimated to be ~6 and the quenching constant was 1.4 ns^{-1}. Upon addition of repressor, the quenching rate constant for O_R2 decreases to a value of 1.1 ns^{-1}. The change in DNA conformation upon protein binding is also expected to alter the distance distribution between donor (H258) and acceptor (EtBr) molecules leading to the decrease in k_q. The mean number of EtBr (5–6) intercalated per DNA strand is in good agreement with the stoichiometry of the species involved. In order to get an idea of the probability distance distribution, we analyzed the time-resolved fluorescence decays of DNA bound H258 in presence and absence of EtBr to construct the distance distribution function, $P(r)$ [32]. As evident in Fig. 4, the half width (hw) of the distance distribution changes from 3.5 Å (H258–O_R2–EtBr) to 3 Å (H258–O_R2–EtBr–λ). In case of O_R1, the distance distribution between H258 and EtBr does not change in presence of protein.

3.2. Dynamical studies

At this juncture, it is important to know the local dynamics of water molecules, which actively take part in various biological functions including the recognition process as well as in maintaining the biological activity [23]. As revealed by the various structural studies, H258 remains attached to the both repressor bound and unbound operator DNA and hence can report their environmental dynamics. In order to study the interfacial water dynamics at DNA–protein interface and the relaxation dynamics of water molecules around two different operators DNA, time-resolved fluorescence experiments were carried out. Fig. 5a displays the fluorescence transients (blue to red end) of H258 in O_R1 DNA, in absence and in presence of λ-repressor. Fig. 5b shows the constructed TRES of H258 giving a shift of 1300 cm^{-1} and 1450 cm^{-1} in a 10 ns time window for O_R1 and O_R1–repressor complex respectively, which indicates that H258 in the excited state is stabilized due to the solvation by the minor groove water molecules along with the DNA itself. However, the change in the net spectral shift of H258 for O_R1 and O_R1 repressor complex is insignificant. The corresponding solvation correlation decay profiles are presented in the inset figure. The solvation correlation decay profile of H258 in O_R1, consists decay time constants of 50 ps (35%) and 7 ns (65%). One of the previous femtosecond-resolved studies on the DNA minor grove water dynamics reveals the hydration time scale of 1.4 ps and 20 ps [19]. However, in our limited time resolution (picosecond-resolved), the observed 50 ps

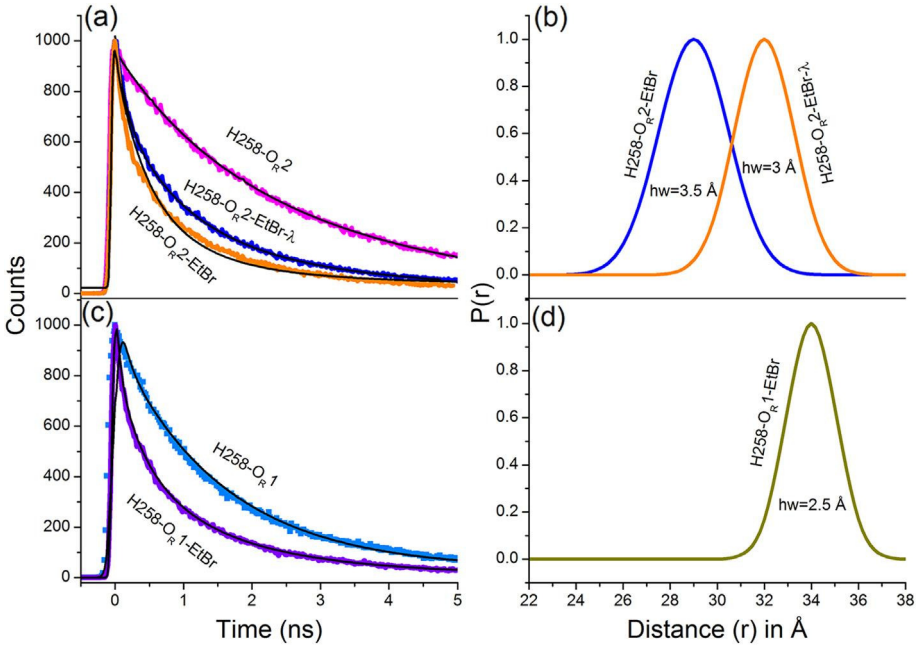

Fig. 4. (a) and (c) Depict the fitting of time-resolved lifetime traces considering the distance distribution between donor and acceptor in O_R2 and O_R1 system respectively. (b) and (d) Show the corresponding probability of distance distribution ($P(r)$) with respect to mean donor–acceptor distance.

component in the solvation decay profile is consistent with the sub-100-ps relaxation of minor groove water molecules [46]. The major decay component of ~10 ns is related to the relaxation of the DNA structure itself [46]. The observed solvation decay constants of H258 are consistent with our earlier studies [47]. Strikingly, the constructed solvation correlation decay for H258 in DNA–protein complex does not change significantly as shown in Fig. 5a (50 ps (30%) and 7 ns (70%)). Fig. 6a displays the fluorescence transients of H258 from blue to red end, i.e. 410 nm, 470 nm, and 530 nm in O_R2 and O_R2–repressor complex. At the blue edge of the spectrum, the fluorescence transient decays on much faster time-scales compared to the transients collected at the red end. Fig. 6b shows the constructed TRES giving a shift of 1200 cm^{-1} and 1350 cm^{-1} in a 10 ns time window for O_R2 and O_R2–repressor complex respectively, essentially indicating that the probe H258 in the excited state is stabilized due to the solvation. As represented in Fig. 7a, the solvation correlation decay function of H258 in O_R2 at room temperature consists of time constants of 50 ps (30%) and 9.0 ns (70%). In presence of λ-repressor (Fig. 7b), the time constant changes to 80 ps (30%) and 11 ns (70%). The unaltered net spectral

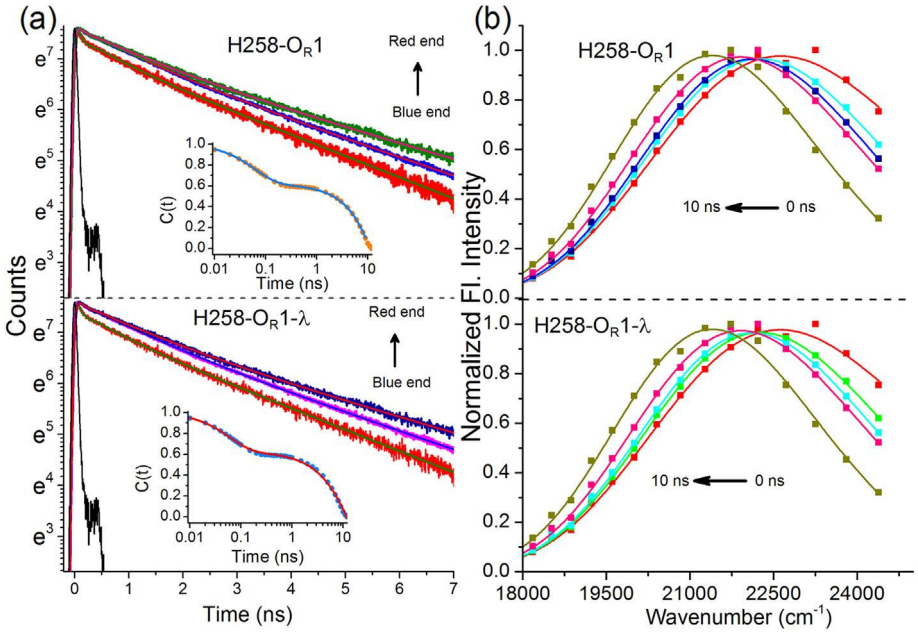

Fig. 5. (a) Picosecond-resolved fluorescence transients of H258 at three wavelengths in O_R1 DNA and O_R1–repressor complex respectively are shown. The excitation wavelength was 375 nm. Solid lines indicate exponential numerical fitting of the experimental data points. The insets depict the solvation correlation decay profiles of H258 in O_R1 in absence and in presence of lambda repressor. (b) Time-resolved emission spectrum (TRES) of H258 in O_R1 and O_R1–repressor complex are shown respectively. The lifetime plots are in semi-log format to better visualize the change of the lifetime traces at different wavelengths.

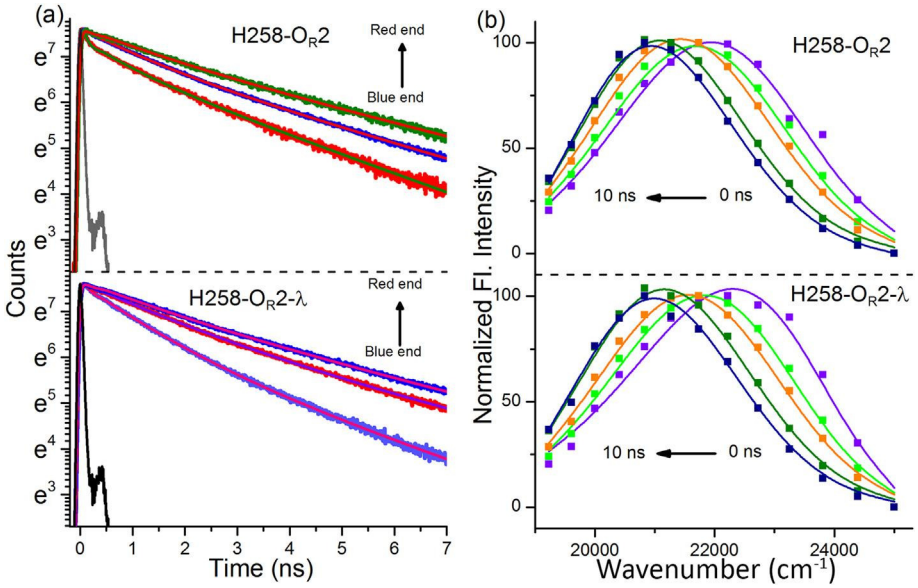

Fig. 6. (a) Picosecond-resolved fluorescence transients of H258 at three wavelengths in O_R2 DNA and O_R2–repressor complex respectively are shown. The excitation wavelength was 375 nm. Solid lines indicate exponential numerical fitting of the experimental data points. (b) Time-resolved emission spectrum (TRES) of H258 in O_R2 and O_R2–repressor complex are shown respectively. The lifetime plots are in semi-log format to better visualize the change of the lifetime traces at different wavelengths.

shift for both DNA and DNA–protein complex is consistent with similar solvation correlation decay profile. Negligible change in the faster time scale of the solvation decay profile is observed suggesting less perturbed water dynamics in the minor groove of DNA (O_R1/O_R2) in presence of repressor. In case of O_R2, the DNA side chain flexibility is slightly hindered as reflected in the slower decay component (9.0 ns changes to 11 ns). However, in case of O_R1, upon repressor binding, side chain flexibility remains unchanged as reflected in the H258 solvation decay profile. Upon repressor binding, the slight change in the slower decay component of H258 solvation decay profile in case of O_R2, could be attributed to the observed conformational change of its structure upon protein binding. In this context, we also attempted to understand whether exchange of minor grove water with the bulk water decreases due to the formation of stable interface in DNA–protein complex. In order to address exchange of minor grove water with the bulk water, we have carried out the temperature dependent TRES analysis of H258 in O_R2 DNA in absence and presence of repressor. Fig. 7a shows the temporal decay of the solvation correlation function ($C(t)$) for the probe (H258) bound to O_R2 at various temperatures. At lower temperature (7 °C), the solvation correlation function decays with a time constant of 40 ps (40%) and 9 ns (60%). With increase in temperature, the contribution of faster solvation decay time gradually decreases and the overall solvation becomes slower. At 40 °C, the temporal decay of the solvation correlation function shows time constants of 40 ps (20%) and 9 ns (80%). On the contrary, for O_R2–repressor complex, the temperature dependent hydration dynamics follows a different course (Fig. 7b). The solvation correlation profile decays with a time constant of 100 ps (30%) and 12.3 ns (70%) at lower temperature (7 °C). In the temperature region of 7 °C–40 °C, the water dynamics in repressor–operator interface is minimally affected as reflected in the solvation correlation decays (Fig. 7b). With further increment of temperature, >50 °C, the water dynamics around H258 changes significantly possibly due to the melting of DNA strand itself. The temperature dependent solvation studies unearth the exchangeability of minor groove water molecules with the bulk water molecules. In the free operator DNA, the exchangeability of minor groove changes with increase in temperature as reflected in the faster solvation decay time. However, due to the formation of a stable interface in the DNA–protein complex, the water molecules in the minor groove are conserved and less susceptible to the temperature changes.

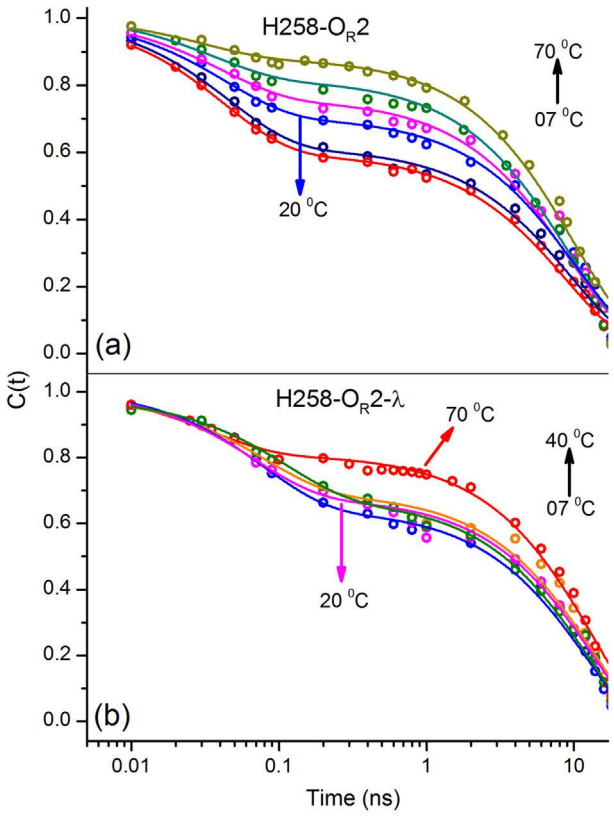

Fig. 7. Temporal decay of the solvation correlation function ($C(t)$) at different temperatures for the H258 in (a) O_R2 and in (b) O_R2–repressor complex. The time has been plotted on a logarithmic scale. Solid lines indicate exponential fitting of the experimental data points.

4. Conclusion

In summary, the study presented here characterizes the conformational change of the DNA, the dynamics of DNA minor groove water molecules and DNA side chain flexibility in a specific DNA protein interaction between λ-repressor and two operators DNA (O_R1 and O_R2). In specific DNA–protein interaction, the recognition process does not only involve the charge and shape complementarities, but also rely upon the dynamics of interfacial water molecules. Our findings indicate the preservation of minor groove water molecules due to formation of stable DNA–protein complex. The dynamics of these DNA minor groove water molecules and the flexibility of DNA side chain is minimally affected upon interaction with the protein as revealed by the excited state relaxation of minor groove binder H258. It has to be noted that, upon protein binding, the slight change in solvent relaxation decay profile of H258 in O_R2 is consistent with the structural modification of the DNA as evidenced from CD and FRET. Our experimental study is expected to contribute towards understanding the role of minor groove water relaxation and DNA side chain flexibility in DNA–protein complex formation.

Acknowledgments

SB and SC thank CSIR (India) for the research fellowships. We thank DST (India) for financial grants (SB/S1/PC-011/2013 and DST/TM/SERI/2k11/103). We are extremely grateful to Professor Siddhartha Roy (Indian Institute of Chemical Biology, Kolkata) for allowing us to work in his laboratory for lambda repressor isolation and purification. We also thank Prof. Roy for his valuable suggestions and encouragement during the entire course of the studies.

References

[1] G. Orphanides, D. Reinberg, A unified theory of gene expression, Cell 108 (2002) 439–451.
[2] C.G. Kalodimos, N. Biris, A.M.J.J. Bonvin, M.M. Levandoski, M. Guennuegues, R. Boelens, R. Kaptein, Structure and flexibility adaptation in nonspecific and specific protein–DNA complexes, Science 305 (2004) 386–389.
[3] C. Muller, P. Calsou, P. Frit, B. Salles, Regulation of the DNA-dependent protein kinase (DNA-PK) activity in eukaryotic cells, Biochimie 81 (1999) 117–125.
[4] A.H. Koop, S.I. Staprans, S. Bourgeois, Specific binding of the cAMP receptor protein of *Escherichia coli* to the lactose operon promoter, Biochimie 67 (1985) 161–175.
[5] R. Rohs, X.S. Jin, S.M. West, R. Joshi, B. Honig, R.S. Mann, Origins of specificity in protein–DNA recognition, Annu. Rev. Biochem. 79 (2010) 233–269.
[6] H.X. Zhou, Rapid search for specific sites on DNA through conformational switch of nonspecifically bound proteins, Proc. Natl. Acad. Sci. U. S. A. 108 (2011) 8651–8656.
[7] Y. Kao-Huang, A. Revzin, A.P. Butler, P. O'Conner, D.W. Noble, P.H. Von Hippel, Nonspecific DNA binding of genome-regulating proteins as a biological control mechanism: measurement of DNA-bound *Escherichia coli* lac repressor in vivo, Proc. Natl. Acad. Sci. U. S. A. 74 (1977) 4228–4232.
[8] D. Zhong, S.K. Pal, A.H. Zewail, Femtosecond studies of protein–DNA binding and dynamics: histone I, Chem. Phys. Chem. 2 (2001) 219–227.
[9] R. Sarkar, S.K. Pal, Interaction of Hoechst 33258 and ethidium with histone 1–DNA condensates, Biomacromolecules 8 (2007) 3332–3339.
[10] C.K. Reddy, A. Das, B. Jayaram, Do water molecules mediate protein–DNA recognition? J. Mol. Biol. 314 (2001) 619–632.
[11] R. Sarkar, S.K. Pal, Ligand–DNA interaction in a nanocage of reverse micelle, Biopolymers 83 (2006) 675–686.
[12] V. Ramakrishnan, R. Rajagopalan, Dynamics and thermodynamics of water around EcoRI bound to a minimally mutated DNA chain, Phys. Chem. Chem. Phys. 14 (2012) 12277–12284.
[13] C.O. Pabo, R.T. Sauer, Protein–DNA recognition, Annu. Rev. Biochem. 53 (1984) 293–321.
[14] N.Y. Sidorova, D.C. Rau, The dissociation rate of the EcoRI–DNA-specific complex is linked to water activity, Biopolymers 53 (2000) 363–368.
[15] B. Nguyen, S. Neidle, W.D. Wilson, A role for water molecules in DNA-ligand minor groove recognition, Acc. Chem. Res. 42 (2009) 11–21.
[16] Z. Otwinowski, R.W. Schevitz, R.G. Zhang, C.L. Lawson, A. Joachimiak, R.Q. Marmorstein, B.F. Luisi, P.B. Sigler, Crystal-structure of Trp repressor operator complex at atomic resolution, Nature 335 (1988) 321–329.
[17] S. Jones, P. van Heyningen, H.M. Berman, J.M. Thornton, Protein–DNA interactions: a structural analysis, J. Mol. Biol. 287 (1999) 877–896.
[18] S.K. Pal, A.H. Zewail, Dynamics of water in biological recognition, Chem. Rev. 104 (2004) 2099–2124.
[19] S.K. Pal, L.A. Zhao, A.H. Zewail, Water at DNA surfaces: ultrafast dynamics in minor groove recognition, Proc. Natl. Acad. Sci. U. S. A. 100 (2003) 8113–8118.
[20] M. Ptashne, N. Hopkins, The operators controlled by the lambda phage repressor, Proc. Natl. Acad. Sci. U. S. A. 60 (1968) 1282–1287.
[21] A.D. Johnson, B.J. Meyer, M. Ptashne, Interactions between DNA-bound repressors govern regulation by the λ phage repressor, Proc. Natl. Acad. Sci. U. S. A. 76 (1979) 5061–5065.
[22] R.T. Sauer, K. Hehir, R.S. Stearman, M.A. Weiss, A. Jeitler-Nilsson, E.G. Suchanek, C.O. Pabo, An engineered intersubunit disulfide enhances the stability and DNA binding of the N-terminal domain of lambda repressor, Biochemistry 25 (1986) 5992–5998.
[23] T. Mondol, S. Batabyal, A. Mazumder, S. Roy, S.K. Pal, Recognition of different DNA sequences by a DNA-binding protein alters protein dynamics differentially, FEBS Lett. 586 (2012) 258–262.
[24] S. Deb, S. Bandyopadhyay, S. Roy, DNA sequence dependent and independent conformational changes in multipartite operator recognition by lambda-repressor, Biochemistry 39 (2000) 3377–3383.
[25] T. Mondol, S. Batabyal, S.K. Pal, Ultrafast electron transfer in the recognition of different DNA sequences by a DNA-binding protein with different dynamical conformations, J. Biomol. Struct. Dyn. 30 (2012) 362–370.
[26] P.E. Pjura, K. Grzeskowiak, R.E. Dickerson, Binding of Hoechst 33258 to the minor groove of B-DNA, J. Mol. Biol. 197 (1987) 257–271.
[27] S. Sen, D. Andreatta, S.Y. Ponomarev, D.L. Beveridge, M.A. Berg, Dynamics of water and ions near DNA: comparison of simulation to time-resolved Stokes-shift experiments, J. Am. Chem. Soc. 131 (2009) 1724–1735.
[28] R. Saha, U. Banik, S. Bandopadhyay, N.C. Mandal, B. Bhattacharyya, S. Roy, An operator-induced conformational change in the c-terminal domain of the lambda-repressor, J. Biol. Chem. 267 (1992) 5862–5867.
[29] C.O. Pabo, R.T. Sauer, J.M. Sturtevant, M. Ptashne, The lambda repressor contains two domains, Proc. Natl. Acad. Sci. U. S. A. 76 (1979) 1608–1612.
[30] C. Brack, V. Pirrotta, Electron microscopic study of the repressor of bacteriophage lambda and its interaction with operator DNA, J. Mol. Biol. 96 (1975) 139–152.
[31] S. Bandyopadhyay, C. Mukhopadhyay, S. Roy, Dimer–dimer interfaces of the λ-repressor are different in liganded and free states†, Biochemistry 35 (1996) 5033–5040.
[32] J.R. Lakowicz, Principles of Fluorescence Spectroscopy, Kluwer Academic/Plenum, New York, 2006.
[33] B.P. Maliwal, J. Kusba, J.R. Lakowicz, Fluorescence energy-transfer in one-dimension – frequency-domain fluorescence study of DNA-fluorophore complexes, Biopolymers 35 (1995) 245–255.
[34] D.V. O'Connor, D. Philips, Time Correlated Single Photon Counting, Academic, London, 1984.
[35] M.L. Horng, J.A. Gardecki, A. Papazyan, M. Maroncelli, Subpicosecond measurements of polar solvation dynamics: coumarin 153 revisited, J. Phys. Chem. 99 (1995) 17311–17337.
[36] M. Tachiya, Kinetics of quenching of luminescent probes in micellar systems. II, J. Chem. Phys. 76 (1982) 340–348.
[37] J.M. Zemke, B.C. Daglen, M. Tachiya, D.R. Tyler, Applications of the Tachiya fluorescence quenching model to describe the kinetics of solid-state polymer photodegradation, Macromolecules 44 (2011) 6625–6628.
[38] S. Sadhu, M. Tachiya, A. Patra, A Stochastic model for energy transfer from CdS quantum dots/rods (donors) to nile red dye (acceptors), J. Phys. Chem. C 113 (2009) 19488–19492.
[39] S. Batabyal, T. Mondol, S.K. Pal, Picosecond-resolved solvent reorganization and energy transfer in biological and model cavities, Biochimie 95 (2013) 1127–1135.
[40] T. Mondol, P. Rajdev, A. Makhal, S.K. Pal, Interaction of an antituberculosis drug with a nanoscopic macromolecular assembly: temperature-dependent Förster resonance energy transfer studies on rifampicin in an anionic sodium dodecyl sulfate micelle, J. Phys. Chem. B 115 (2011) 2924–2930.
[41] Y. Lyubchenko, L. Shlyakhtenko, B. Chernov, R.E. Harrington, DNA bending induced by Cro protein-binding as demonstrated by gel-electrophoresis, Proc. Natl. Acad. Sci. U. S. A. 88 (1991) 5331–5334.
[42] D. Banerjee, S.K. Pal, Simultaneous binding of minor groove binder and intercalator to dodecamer DNA: importance of relative orientation of donor and acceptor in FRET, J. Phys. Chem. B 111 (2007) 5047–5052.
[43] T. Mondol, S. Batabyal, S.K. Pal, Interaction of an antituberculosis drug with nano-sized cationic micelle: Förster resonance energy transfer from dansyl to rifampicin in the microenvironment, Photochem. Photobiol. 88 (2012) 328–335.
[44] M. Tachiya, Application of a generating function to reaction kinetics in micelles. Kinetics of quenching of luminescent probes in micelles, Chem. Phys. Lett. 33 (1975) 289–292.
[45] S. Banerjee, M. Tachiya, S.K. Pal, Caffeine-mediated detachment of mutagenic ethidium from various nanoscopic micelles: an ultrafast Förster resonance energy transfer study, J. Phys. Chem. B 116 (2012) 7841–7848.
[46] E.B. Brauns, M.L. Madaras, R.S. Coleman, C.J. Murphy, M.A. Berg, Measurement of local DNA reorganization on the picosecond and nanosecond time scales, J. Am. Chem. Soc. 121 (1999) 11644–11649.
[47] D. Banerjee, S.K. Pal, Direct observation of essential DNA dynamics: melting and reformation of the DNA minor groove, J. Phys. Chem. B 111 (2007) 10833–10838.